Modeling of Mass Transfer in Combination with a Homogeneously Catalyzed Reaction

J. A. A. Hoorn
DSM Research, P.O. Box 18, 6160 MD Geleen, Netherlands

G. F. Versteeg
Dept. of Chemical Engineering, University of Twente, P.O. Box 217, 7500 AE Enschede, Netherlands

DOI 10.1002/aic.10869
Published online April 21, 2006 in Wiley InterScience (www.interscience.wiley.com).

The mass transfer rates of a gaseous reactant into a liquid where the reactions are catalyzed by homogeneous catalysts have been evaluated by the numerical solution of the diffusion-reaction equations according to Higbie's penetration theory. The concentration profiles as well as enhancement factors are discussed as functions of the kinetic rate constants and the diffusion coefficients of the catalytic intermediates. In addition to the complex catalytic model, two simplified models were applied in order to facilitate design calculations. One version was obtained by application of the Bodenstein approximation; the simplest version comprised only the stoichiometric reaction. The Bodenstein model provides a very good approximation except for deviating diffusion coefficients of the catalytic intermediates. The applicability of the stoichiometric model is not as wide as with the Bodenstein model, but for some conditions acceptable approximations are achieved. © 2006 American Institute of Chemical Engineers *AIChE J,* 52: 2551–2564, 2006
Keywords: diffusion, reaction, model, homogeneous catalysis, enhancement factor, design

Introduction

Homogeneous catalysis is broadly applied in the process industry and has been extensively studied in academia. Although the mechanisms of a large number of systems have been extensively studied, the complexity of a complete catalytic network means that the kinetic expressions and parameters have been defined for only a limited number of systems.

Halpern et al.[1-3] present one of the few examples where the detailed kinetics of a homogeneously catalyzed system have been elucidated via a combination of analytical techniques and kinetic experiments. The scheme presented in Figure 1 has been adapted from Halpern.[1] In many other studies on hydrogenation systems, the kinetic rate expressions are determined for the overall reactions.[4] Reaction rates in Figure 1 are respectively expressed as first order in the specific catalyst intermediate and first order in the reactant where appropriate. The kinetic constants in the rate expressions have been determined from measurements. The rate constants in Figure 1 are partly derived from spectrally determined equilibrium constants; therefore, in the case of k_{-1}, a minimum is given rather than an exactly measured value.

Another example where the kinetics of the individual reaction steps have been studied in detail is in the catalytic cycle of iron chelate complexes. In these catalytic cycles, nitrous and sulphur oxides are absorbed in water, NO is reduced, and the produced sulphite is oxidized.[5] Main products are a series of nitrogen and sulphur containing components (Figure 2). The differences in reaction rates indicated with slow or fast in Figure 2 are orders of magnitude. The second order rate constant of the reaction of NO with Fe^{II}(EDTA) is higher than $6{\cdot}10^7$ l/mol/s whereas the reduction of Fe^{III}(EDTA) by sulphite

Correspondence concerning this article should be addressed to J. A. A. Hoorn at johan.hoorn@dsm.com.

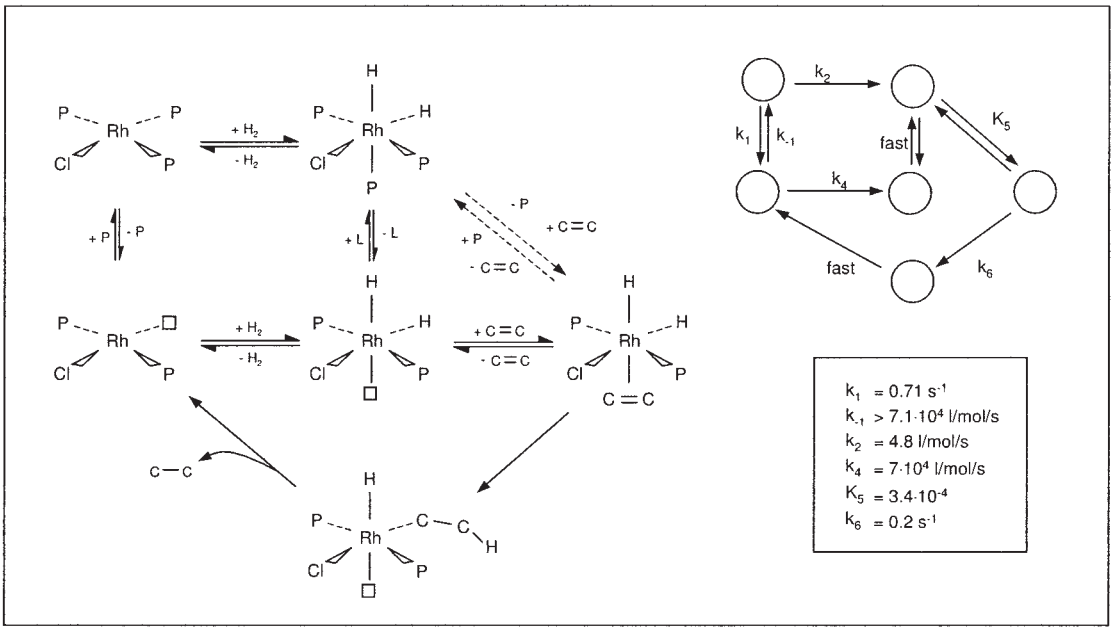

Figure 1. Part of the catalytic cycle of a rhodium catalyzed hydrogenation.

The upper right part indicates the reaction rate constants that have been quantitatively identified. P indicates PPh_3.

proceeds much slower. Given a first order reaction rate constant of $4 \cdot 10^{-5}\ s^{-1}$ as observed for 0.05 mol/l sulphite solution, the derived (pseudo) second order rate constant is equivalent to $8 \cdot 10^{-4}$ l/mol/s, indicating a difference of 10^{11} with the former reaction.

Despite the occurrence of very fast reactions in solution for the majority of homogeneously catalyzed reactions described in literature, the aspects of mass transfer and mass transfer limitations are only briefly addressed. Very frequently reaction conditions are chosen in such a way that limitations are avoided.[6] On some occasions, the mass transfer rates of the gaseous components are taken into account by application of mass transfer coefficients.[7] The influence of mass transfer on the stability of a hydroformylation reactor has been investigated by van Elk et al.[8] The kinetic model applied in this study was an overall empirical rate expression. The calculation of the rate of mass transfer in the absorption of gases followed by (complex) chemical reactions is one of the key issues in the design and scale-up of gas-liquid reactors. In textbooks as well as in practice, the simplification of a reaction network to a single first-order irreversible reaction is often applied. This approach has the advantage of simple concepts of Hatta number and enhancement factor. A great number of researchers have extended the analytical solutions for other than first order irreversible reactions. The spectrum of reactive systems includes single and multiple reactions (parallel and in-series), irreversible as well as reversible reactions, and auto catalytic reactions.

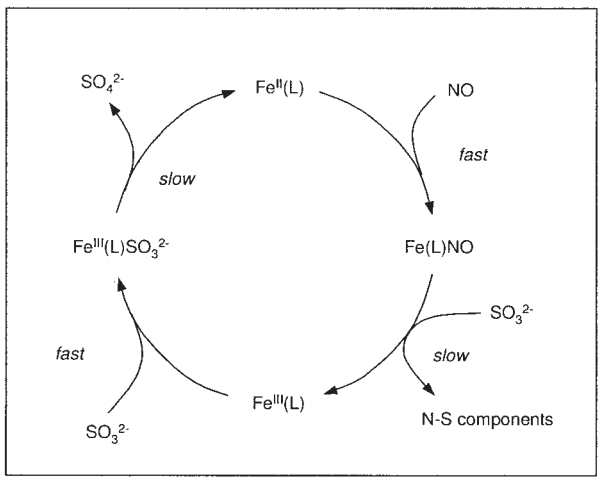

Figure 2. Main catalytic cycle of simultaneous absorption and reaction of nitrous and sulphur oxides.

The ligand L is a chelating component like EDTA.

A comprehensive overview on the literature on mass transfer accompanied by complex chemical reactions can be found in an article by Van Swaaij and Versteeg.[9] An early numerical study on homogeneously catalyzed gas-liquid reactions in combination with mass transfer effects is presented by Ponzi and Lemcoff.[10] They studied a reaction system comprising absorption of two gases—one gaseous reactant and one component for the regeneration of the catalyst as is applied in, for example, the production of acetaldehyde from ethene (Wacker process).

There are a number of reasons to study the combination of homogeneously catalyzed reactions in the mass transfer limited regime. As industrial conditions in reactors often deviate from laboratory experimental set-ups, it is likely that in plant reactors conditions occur where mass transfer limitations influence the performance of the reactor. In addition, mass transfer limitations are often difficult to separate from "ordinary" kinetic observations. It is, therefore, very well possible that in a number of laboratory reactors, mass transfer limitations have

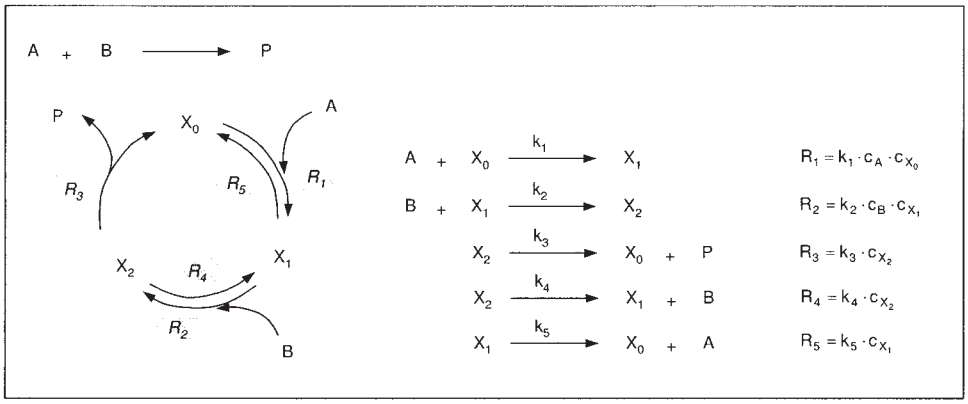

Figure 3. Components and reactions in the HC model.

been erroneously left out of consideration. Therefore, a general method to incorporate the transport equations with the elementary reactions would be very helpful. Once a fundamental model has been established, it is interesting to determine the conditions where a simplified model provides results close to the fundamental model. The simplified model is more applicable in, for example, design studies, plant simulations, and for control purposes. This approach has been recently exercised in a diffusion-reaction system involving radical intermediates.[11]

Mass Transfer and Reaction Model

Three models are considered in this article. All models comprise A as a gaseous component from the gas phase transferring to the liquid and reacting with B to form product P. The models differ in the reaction pathways and their association with a reaction rate expression.

ABP model

This is the stoichiometric model for the reaction A + B → P. The reaction rate is defined as:

$$R_i = \nu_i \cdot k_1 \cdot c_A \cdot C_B \tag{1}$$

with $\nu_i = -1$ for I = A,B and $\nu_i = 1$ for I = P.

The Hatta number for this type of reaction is defined by:

$$\varphi = \frac{\sqrt{k_1 \cdot c_B \cdot D_A}}{k_L} \tag{2}$$

HC model

This model is a representation of the reaction proceeding through homogeneous catalysis in which a minimum of catalyst intermediates is involved. The reactions and notation are indicated in Figure 3, along with the expressions for the reaction rates.

The catalyst complexes in the reactions are noted by X_i where i = 0 to 2. The index zero is to identify the stable catalyst configuration being the dominant species in the bulk of the liquid. Although the reaction cycle shown in Figure 3 comprises several equilibria, the overall sequence reflects essentially an irreversible reaction. For the reversible reactions between X_0 and X_1 and between X_1 and X_2, the following equilibrium constants are defined:

$$K_{15} = \frac{k_1}{k_5} = \frac{c_{X_1}}{c_{X_0} \cdot c_A}$$

$$K_{24} = \frac{k_2}{k_4} = \frac{c_{X_2}}{c_{X_1} \cdot c_B} \tag{3}$$

The reaction rate for each component is the summation of all the rates of the reactions involving the component, taking into account the stoichiometric coefficient. The reaction rates are given in Figure 3.

Bo model

Assuming a single reaction as in model ABP, the reaction rate expression is derived from the HC model by a Bodenstein approximation in order to eliminate the concentrations of the catalytic intermediates. There are many options and assumptions to arrive at simplified expressions[12]; here the choice has been made to assume quasi-stationary behavior of the catalytic intermediates (for details, see Appendix). Reduction of the network in Figure 3 to the single reaction A + B → P gives the reaction rate expression:

$$R_i = \frac{\nu_i \cdot \dfrac{k_1 \cdot k_2 \cdot k_3}{k_5 \cdot (k_3 + k_4)} \cdot c_{cat} \cdot c_A \cdot c_B}{1 + \dfrac{k_1}{k_5} \cdot c_A + \dfrac{k_2 \cdot k_3}{k_5 \cdot (k_3 + k_4)} \cdot c_B + \dfrac{k_1 \cdot k_2}{k_5 \cdot (k_3 + k_4)} \cdot c_A \cdot c_B} \tag{4}$$

with $\nu_i = -1$ for i = A,B and $\nu_i = 1$ for i = P.

The total catalyst concentration c_{cat} is assumed to be constant, and the kinetic constants in this Eq. 4 are identical to the constants in Figure 3.

Absorption model

To reduce the number of variables studied in the previously defined models, a number of assumptions have been made:

- diffusion is described by Fick's laws; there are no convective contributions in the liquid phase to mass transport,
- the solvent is inert,
- the temperature is constant; heat effects of reactions and absorption are not included,
- the density of the liquid is constant,
- mass transfer resistance in the gas phase is negligible.
- For the description of mass transfer, the penetration theory according to Higbie is applied. The disadvantage of more complicated numerical calculations in the penetration theory in comparison to the film theory is compensated by more physically realistic descriptions.[13] In the penetration theory, the equation for a single diffusing and reacting component (i) is given by:

$$\frac{\partial c_i}{\partial t} = D_i \cdot \frac{\partial^2 c_i}{\partial X^2} + R_i \tag{5}$$

$$\text{Initial condition: } t = 0 \quad \text{and} \quad x \geq 0 \qquad c_i = c_{i,bulk} \tag{6}$$

$$\text{Boundary conditions: } t > 0 \quad \text{and} \quad x = \infty \qquad c_i = c_{i,bulk} \tag{7}$$

$$t > 0 \quad \text{and} \quad x = 0 \qquad c_i = c_i^* \tag{8}$$

All concentration profiles and derived properties are evaluated at the end of the contact time, τ_p. The contact time for absorption according to the penetration model is related to the liquid mass transfer coefficient and the diffusion coefficient of component A:

$$\tau_p = 4 \cdot \frac{D_A}{\pi \cdot k_L^2} \tag{9}$$

The x-axes in the graphs representing concentration profiles are scaled. The reference scale is based on the solution of the penetration model for an absorption of a single component without reaction.[14] (In Eq. 10, c_A^* indicates the interfacial concentration.)

$$c_A(x, t) = c_A^* \cdot \left[1 - \text{erf}\left(\frac{x}{2\sqrt{D_A \cdot t}}\right)\right] \tag{10}$$

The penetration depth (δ_p) is defined as:

$$\delta_p = 4 \cdot \frac{D_A}{k_L} \tag{11}$$

This definition is obtained when δ_p and τ_p substituted in the error function of Eq. 10 equal the square root of pi:

$$\frac{\delta_p}{2\sqrt{D_A \cdot \tau_p}} = \sqrt{\pi} \tag{11}$$

Table 1. Default Parameter Values for Model Simulation

Model	Component	Gas Phase Concentration C_g (kmol/m^3)	Liquid Phase Concentration C (kmol/m^3)	Solubility Coefficient mgl (−)
ABP, Bo	A	1	10^{-40}	3
	B	10^{-40}	2	10^{40}
	P	10^{-40}	10^{-40}	10^{40}
HC	A	1	10^{-40}	3
	B	10^{-40}	2	10^{40}
	P	10^{-40}	10^{-40}	10^{40}
	X_0	10^{-40}	0.0001	10^{40}
	X_1	10^{-40}	10^{-40}	10^{40}
	X_2	10^{-40}	10^{-40}	10^{40}

For $\sqrt{\pi}$ the error function is close to zero and fits well with the definition of the contact time, Eq. 9.

A method presented by Cornelisse et al.[15] is applied to solve the system of coupled non-linear parabolic partial differential equations. This approach is based on a three-point backward scheme for finite-differencing originally proposed by Baker and Oliphant.[16] For an efficient use of grid point allocation, transformation of both the time and spatial variables has been applied.[17] Further details on the implementation of the numerical methods can be found in Hoorn et al.[11] The boundary conditions at $x = \infty$ are approximated by extending the grid to a depth in the liquid sufficiently larger than the penetration depth as defined by Eq. 12. Taking the range of the depth in the liquid as 5 times the penetration depth is assumed to be sufficient. This assumption is checked for each model calculation by inspection of the gradients near $x = 5 \cdot \delta_p$. The gas phase concentration is constant for a contact period τ_p; therefore, the enhancement factor regarding component A is calculated according to:

$$E = \frac{\int_0^{\tau_p} -D \cdot \frac{dc_A}{dx}\big|_{x=0}\, dt}{k_L \cdot \tau_p \cdot (c_{A|_{x=0}} - c_{A,bulk})} \tag{13}$$

The gradient at $x = 0$ is determined by fitting a cubic spline through the first 20 grid points from the interface. The integral from 0 to τ_p is approximated by the summation of the gradients over all time steps (trapezium rule).

The reaction rate constants and diffusion coefficients have been varied. The default reaction rate constants are $k_i = 10^5$ m^3/kmol/s ($i = 1,2$) and $k_i = 10^6$ s^{-1} ($i = 3,4$, or 5). All diffusion coefficients have default values of $1 \cdot 10^{-9}$ m^2/s. Other parameter values have been kept constant to keep the number of variations within reasonable proportions. The gas phase concentrations and gas-liquid partition coefficients were kept constant, as well as the liquid phase concentrations at $t = 0$ and in the liquid bulk. The liquid side mass transfer coefficient k_l has been fixed at $5 \cdot 10^{-5}$ m/s as a typical value for gas-liquid reactors. All default input parameters are listed in Table 1. The number of spatial grid points has been set to 800 for all simulations. The number of grid points for the time coordinates was set to 600.

For displaying convenient values in graphs, the concentrations are scaled. Components B and P are scaled by the initial concentration of B, whereas A is scaled with the equilibrium interface concentration of A (all indicated with c_0). The cata-

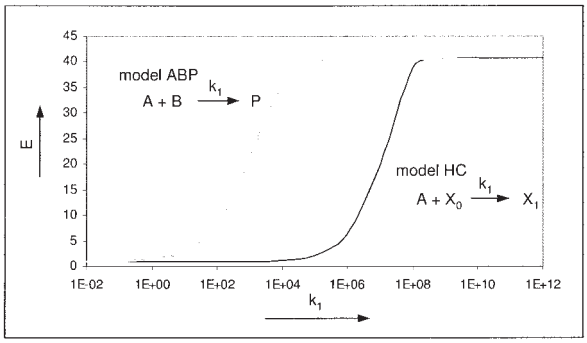

Figure 4. Enhancement factor as a function of the rate constant for the HC and ABP models.

lytic intermediates are scaled by the total catalyst concentration (c_0 or $c_{x,0}$).

Simulation Results

Irreversible reaction system

For small reaction rate constants for reactions 4 and 5 in the HC model, that is, $k_i = 10^{-2}$ s^{-1}, the reaction cycle shown in Figure 3 can be regarded as completely irreversible. The calculated enhancement factor as a unction of k_1 with k_2 and k_3 fixed to values of 10^{10} is shown in Figure 4. The results obtained by application of the ABP-model are also plotted in Figure 4. The enhancement factor at infinitely fast reaction is for both models equal to 40.8. The almost constant difference in k_1 between the HC and the ABP models for equal values of E (Figure 4) corresponds to the concentration of the initial total catalytic intermediate concentration, such as k_1(ABP) = $c_{x,0}$·k_1(HC). A few concentration profiles corresponding to points in Figure 4 for the HC model are given in Figure 5. Already at low values for k_1, the absorption of A is enhanced but there is not much effect on the profiles of B and P (Figure 5a). Concentrations of B are non-zero throughout the penetration depth, and the concentration gradients for P are quite small. All catalytic species are in the form of X_0. When A diffuses into the liquid, it reacts with X_0 to form X_1; but as the succeeding reactions are (much) faster, X_0 is formed very quickly again out of X_1 via X_2 (not present in significant amounts). Upon increasing the value to $k_1 = 10^7$ m^3/kmol/s, the concentration of B near the interface is gradually reduced and the concentration of P increases (Figure 5b). The ratios between the catalytic intermediates remain unaffected. Increas-

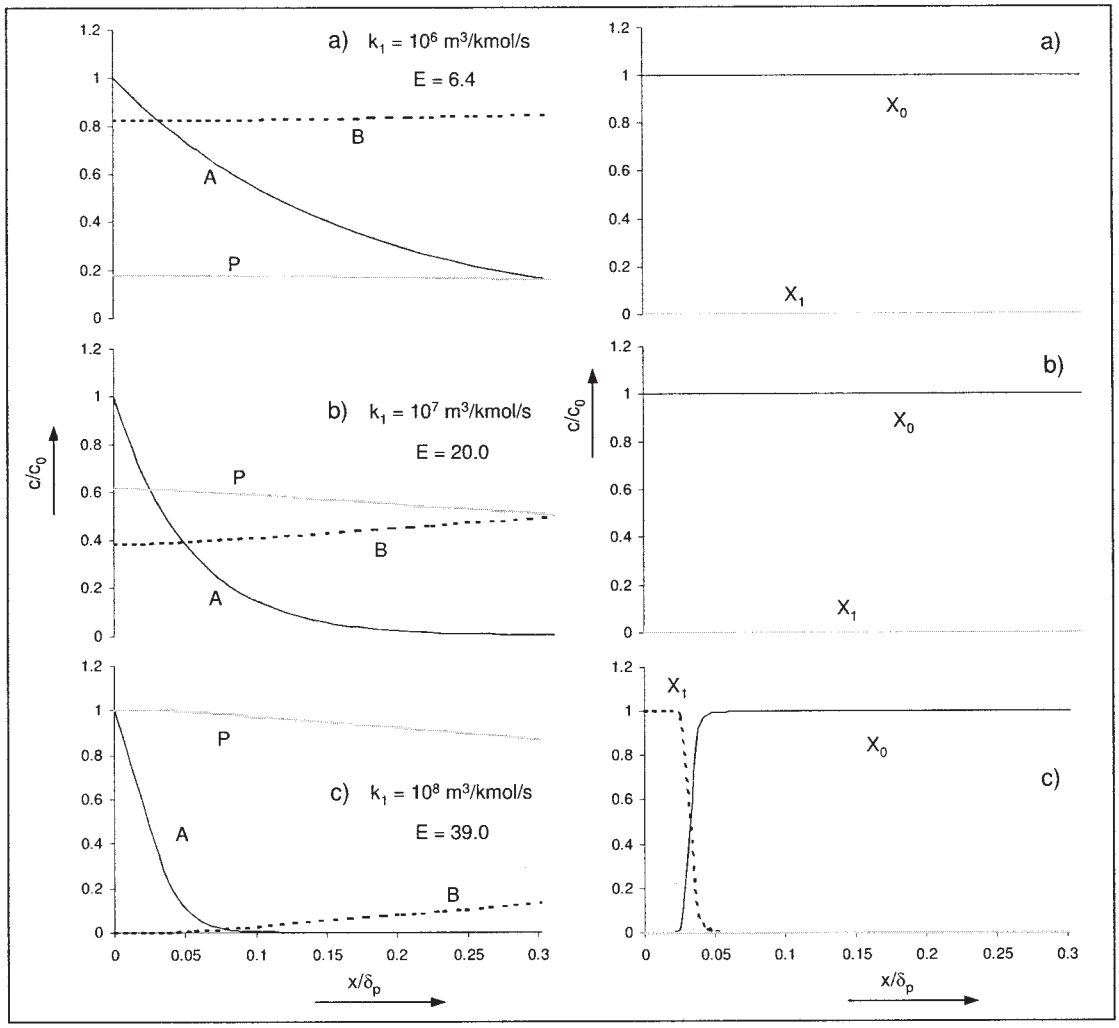

Figure 5. Concentration profiles at the end of the contact time τ_p for different values of k_1.

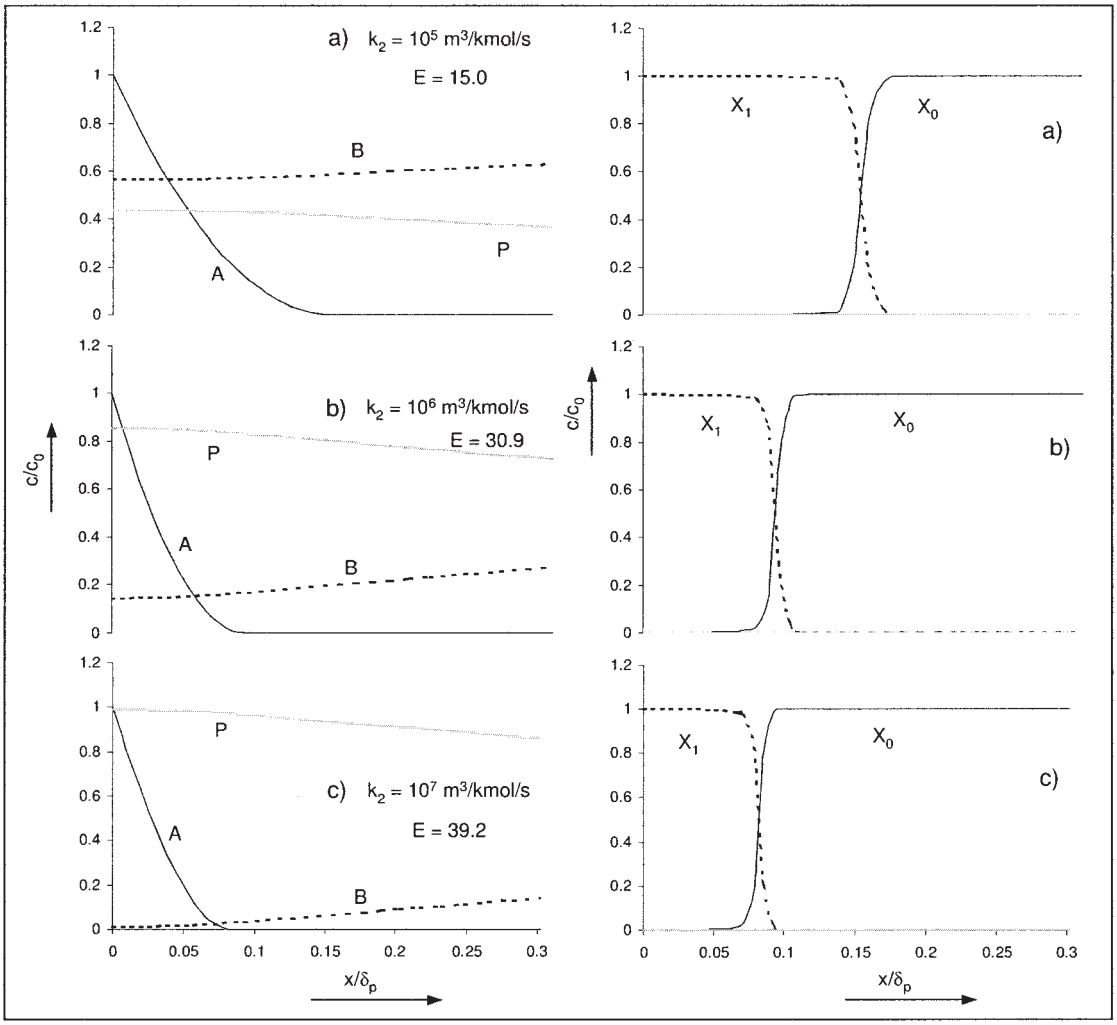

Figure 6. Concentration profiles at the end of the contact time τ_p for different values of k_2.

ing k_1 by another factor of 10, the enhancement factor for A approaches the value for infinitely fast reaction: 39.0 compared to 40.8. In this situation, the concentration of B near the interface is practically zero and X_1 is the dominant catalytic intermediate in this region (Figure 5c). The intermediate X_2 is still only present in very low concentrations all through the liquid because the reaction to X_0 remains very fast (high value for k_3). For values of k_1 higher than 10^8 m³/kmol/s, the profiles do not change a lot; the enhancement factor increases gradually with k_1 to the limit value of 40.8.

With the same parameter set as applied in Figure 5 and varying k_2 instead of k_1 (k_1 fixed at 10^{10} m³/kmol/s), the results are comparable to those in Figure 5. The enhancement factor at high reaction rate is almost identical: 40.7. The profiles for A, B, and P are similar and the concentrations of X_2 are also low. The ratio between X_0 and X_1 is different, however (Figure 6). In Figure 6 it is clear that with all k_2 values, two regions in the penetration area are present with different intermediates as the dominant species. As k_2 increases, the front between X_0 and X_1 does not change in shape but the position in the liquid is shifted towards the G/L interface (Figures 6a and 6b). Because of the high value for k_3, the intermediate X_2 is rapidly converted to X_0 and, therefore, concentrations of X_2 are low throughout the liquid. In the area where A diffuses into the liquid, X_0 reacts with A to form X_1; hence, X_1 is the dominant reactive intermediate near the interface. The bulk of the liquid contains only X_0 so there has to be a location where the ratio of the two intermediates is inverted. By increasing k_2, the reaction rate towards X_0 (via X_2) is increased, thereby shifting the concentration profiles of A as well as X_0 towards the interface.

The concentration of X_2 can have noticeable values when k_3 is varied and k_1 and k_2 are kept constant at 10^{10} m³/kmol/s; see Figure 7. The maximum attainable enhancement factor at high reaction rate is also 40.7. In Figure 7a (low values of k_3), the dominant intermediates are X_0 and X_2 since by the high value of k_2 X_1 reacts very fast to X_2 while the concentration of B is sufficiently high. For high values of k_3, the concentration of X_2 becomes low because the conversion of X_2 into X_0 is increased while the formation of X_2 is decreased because the concentration of B is reduced at the same time (Figure 7c). For intermediate values of k_3, the circle is more balanced, leading to the occurrence of all the three intermediates (Figure 7b). The flux of A as a function of k_3, as shown in Figure 8, is similar in shape to the enhancement factor (Figure 4). This is expected from Eq. 13 since k_L and Δc have equal values in calculating the enhancement factor and the flux.

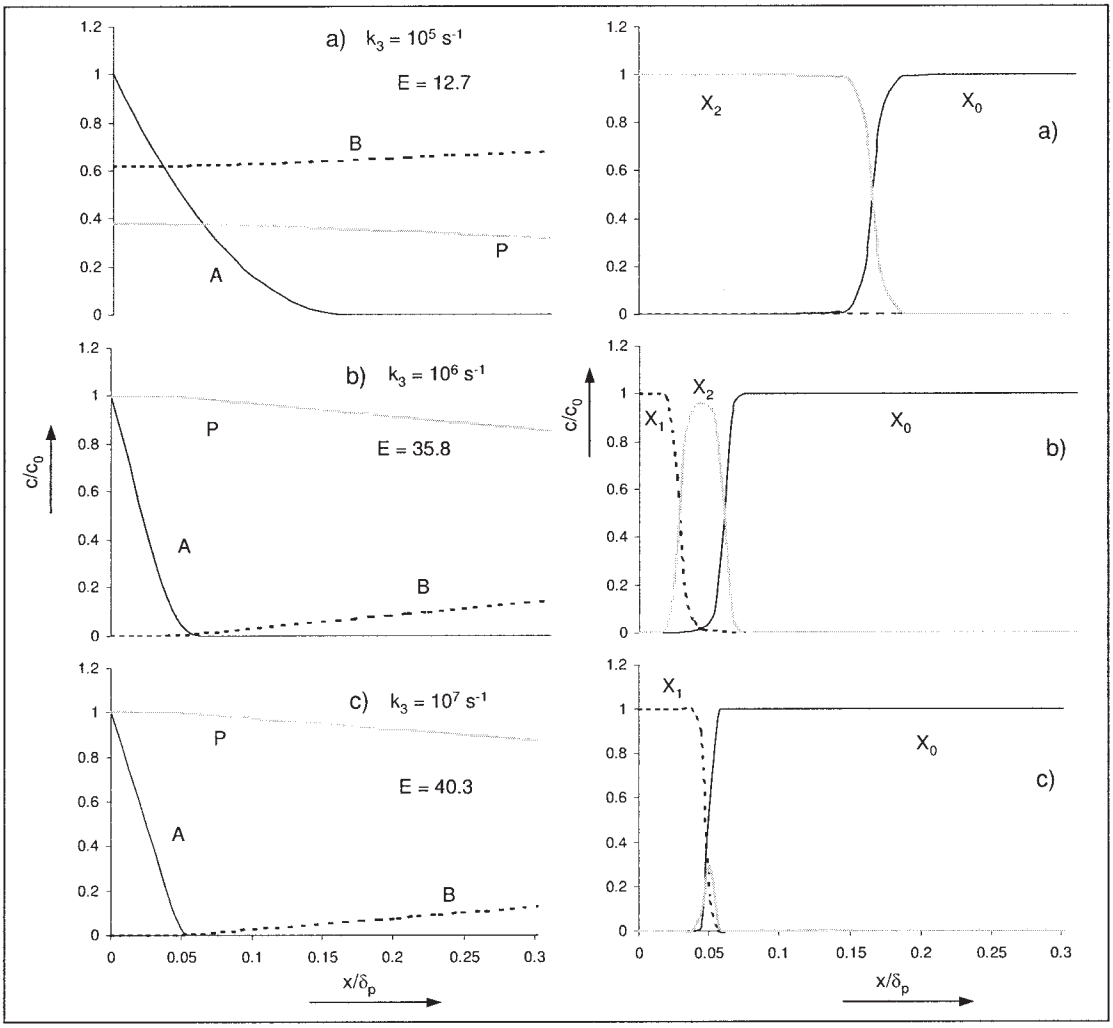

Figure 7. Concentration profiles at the end of the contact time τ_p for different values of k_3.

The shape of the catalytic intermediate profiles is affected by differences in diffusivity of the intermediates. A number of case studies with varying diffusion coefficients were evaluated on the basis of a single set of kinetic parameters (k_1,k_2 = 10^{10} m^3/kmol/s, k_3 = 10^{10} s^{-1}, k_4,k_5 = 10^{-2} s^{-1}). In Figure 9 the concentration profiles for the intermediates are shown where

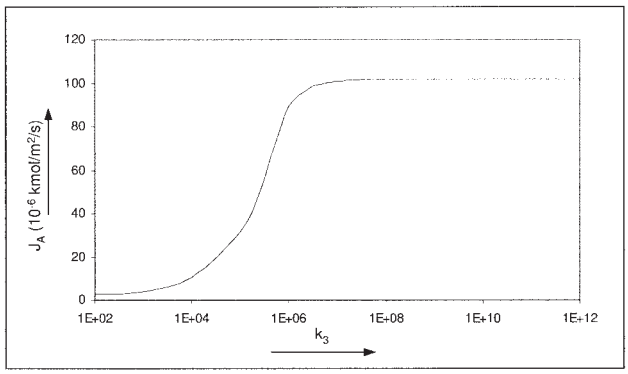

Figure 8. Flux of A across the G/L interface as a function of k_3.

the diffusion coefficients of three intermediates have been alternating set to a lower value while keeping the others at default. Note that the scaling of the c/c_0-axis in Figure 9 is not equal to the preceding Figures. The catalytic intermediate with the lowest diffusion coefficient locally builds up a concentration that is higher than the initial total concentration of catalyst. The shifts in the positions of the switches between the catalytic intermediates suggest that also in the enhancement factors differences might occur. For the default case as well as with $D_c(X_1)$ = 10^{-10} m^2/s (Figures 9a and 9c), the enhancement factor is equal to 35.8. With $D_c(X_0)$ = 10^{-10} m^2/s, the enhancement factor is significantly lowered to E = 15.1. In contrast, the lowering of $D_c(X_2)$ to 10^{-10} m^2/s results in an increase in the enhancement factor to E = 40.0. The observation that with $D_c(X_1)$ = 10^{-10} m^2/s (Figure 9c) the enhancement factor is identical to the default case is not surprising since X_1 as the dominant species near the G/L interface is not involved in the reaction with A. The decrease in E with $D_c(X_0)$ = 10^{-10} m^2/s is caused by the reduction in concentration near the G/L interface (Figure 9b). The intermediates X_1 and X_2 diffuse in the direction of the bulk of the liquid; at the point where A diminishes to zero, the reaction cycle stops at X_0

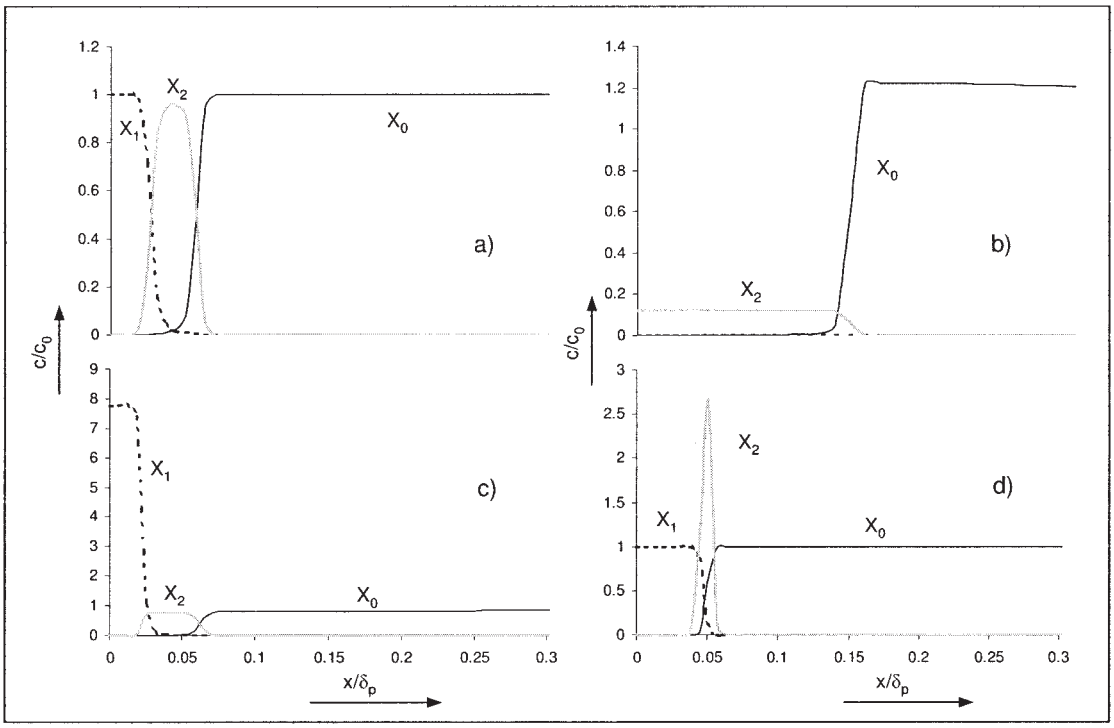

Figure 9. Concentration profiles at the end of the contact time τ_p with varying diffusion coefficients.

(a) Default; (b) $D_c(X_0) = 10^{-10}$ m^2/s; (c) $D_c(X_1) = 10^{-10}$ m^2/s; (d) $D_c(X_2) = 10^{-10}$ m^2/s.

and since this intermediate has the lowest diffusion coefficient the diffusion rate of X_0 in the direction of the G/L interface is much smaller than the supply of X in the form of X_1 and X_2. The slight increase in the enhancement factor in the case of $D_c(X_2)$ to 10^{-10} m^2/s is more difficult to address (Figure 9d). Probably the increase in concentration in X_2 is suitably located between X_1 at the G/L interface and X_0 in the liquid bulk, thereby increasing the overall concentration of catalyst in the region where A penetrates into the liquid.

In the alternate situation where the values for diffusion coefficients are chosen higher instead of lower, the effects appear to be quite similar to those shown in Figure 9 but in the details differences exist (see Figure 10). In the case of $D_c(X_0) = 10^{-8}$ m^2/s (Figure 10b), the diffusion of X_0 in the direction of the G/L interface is larger than the diffusion of X_1 and X_2 in the opposite direction; therefore, the concentrations of the latter two intermediates are increased. The enhancement factor is increased with respect to the default case (E = 40.2 versus 35.8). The profile in Figure 10c is a result of the high diffusivity of X_1: near the interface the concentration of X_1 is lowered by the diffusion in the direction of the liquid bulk. This diffusion is not balanced by X_0 and X_2. However, the enhancement factor is hardly affected by the changes in profile. The explanation is identical to the discussion with Figure 9c: since X_1 as the dominant species near the G/L interface is not involved in the reaction, the enhancement of the absorption of A is not affected. The enhancement factor for the profiles in Figure 9d is significantly lower at E = 13.5. Figure 10d ($D_c(X_2) = 10^{-8}$ m^2/s) is quite similar to Figure 9b ($D_c(X_0) = 10^{-10}$ m^2/s). While in both simulations the concentrations of X_1 in the liquid are close to zero, the rate of the catalytic cycle is determined only by X_0 and X_2 and apparently in this situation the ratio between the diffusion coefficients is more important than the absolute values.

Frequently, reaction rate expressions for homogeneously catalyzed systems are simplified by inclusion of the catalyst concentration in the rate constant. As illustration of this method, Figure 11 shows the enhancement factors calculated by the HC model in comparison to the ABP model with application of the transformation $k_1(ABP) = c_{x,0} \cdot k_1(HC)$, as was already mentioned with Figure 4. Figure 11 clearly shows that only for a limited number of system parameters does the simplification on the catalyst concentration lead to acceptable estimations of the absorption rate.

Conclusion concerning irreversible reactions

In a complete irreversible catalytic cycle, the variation of reaction rate constants determines the concentrations of all components including the catalytic intermediates. With the concentration profiles, the enhancement of the absorption can be explained. In addition to the kinetics, also differences in the diffusivity of the catalytic intermediates can be involved. Simplification of systems of homogeneously catalyzed reactions with mass transfer by means of incorporation of the catalyst concentration into the reaction rate constant could easily result in the prediction of erroneous absorption rates.

Effect of reversibility

It is well known from literature that reversibility of reactions has a significant effect on the mass transfer rate of an absorbing reactant.[17] To study this effect quantitatively, the simulations for the HC model where k_3 was varied (results shown in Figure

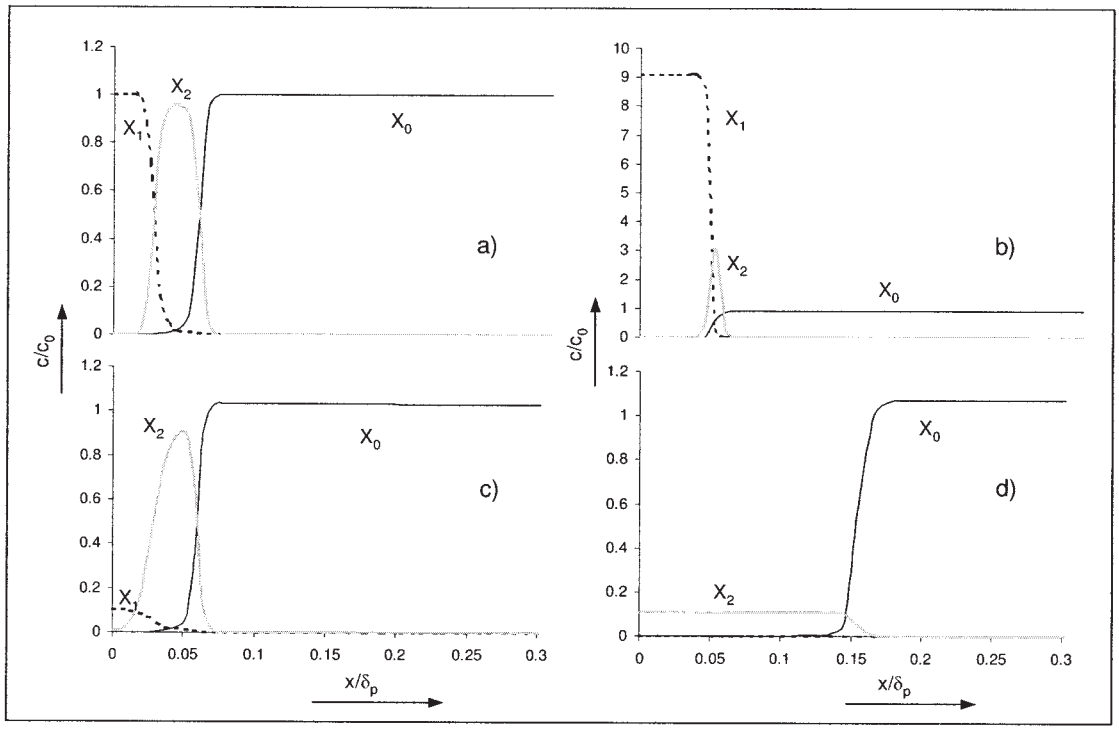

Figure 10. Concentration profiles at the end of the contact time τ_p with varying diffusion coefficients.

(a) Default; (b) $D_c(X_0) = 10^{-8}$ m^2/s; (c) $D_c(X_1) = 10^{-8}$ m^2/s; (d) $D_c(X_2) = 10^{-8}$ m^2/s.

7) were repeated with varying values for k_4 and k_5 (see Figure 12). The rate constants k_1 and k_2 were fixed at 10^{10} m^3/kmol/s and k_4 and k_5 were translated to the corresponding equilibrium constants. In addition, the profiles of the catalytic intermediates for a selected value of k_3 (where the differences in E are maximum) are shown in Figure 13. As is observed from Figure 12 for values of K_{15} and K_{24} between 100 and 10^{12} m^3/kmol, the calculated enhancement factor is not affected. However, with decreasing the equilibrium values below 100 m^3/kmol, significant changes in the simulated values of the enhancement factor occur. Therefore, in line with previously published results,[17] it can be concluded that lower values of the equilibrium constant result in a reduction of the enhancement factor. In Figures 13a and 13d, the concentration profiles of the intermediate components are given for the irreversible (13a) and the reversible case (13d), respectively.

Figure 13a is identical to Figure 7b and so the corresponding profiles for A, B, and P can be found in Figure 7b. These profiles only change gradually when K_{15} and K_{24} are decreased from 10^{12} to 100. The position of the maximum in the concentration of X_2 does not vary either for these simulations. However, it can be seen in Figure 7b that the profiles are less steep and that the species X_0, X_1, and X_2 are occurring simultaneously over a wide range. Figure 13d is the representation of two fast reversible reaction sequences followed by R_3 as the

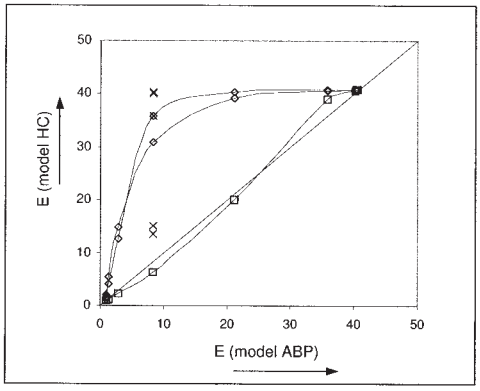

Figure 11. Enhancement factors for the HC model compared to the ABP model with correlation for k_1 by means of catalyst concentration.

Symbols refer to simulations shown in: Figure 5 (□); Figure 6 (◇); Figure 7 (Δ); Figure 9 (×).

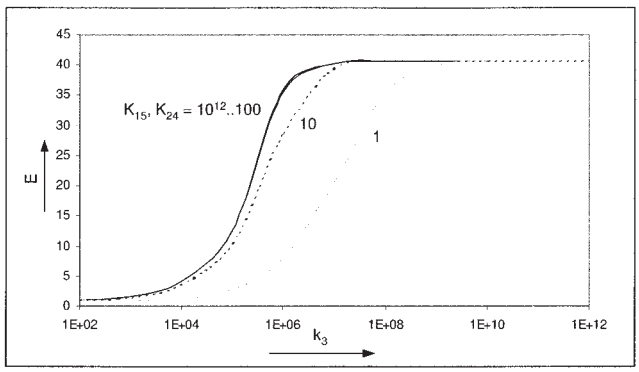

Figure 12. Enhancement factor as function of the rate constant for the reaction $X_2 \rightarrow X_0 + P$ for various equilibrium constants.

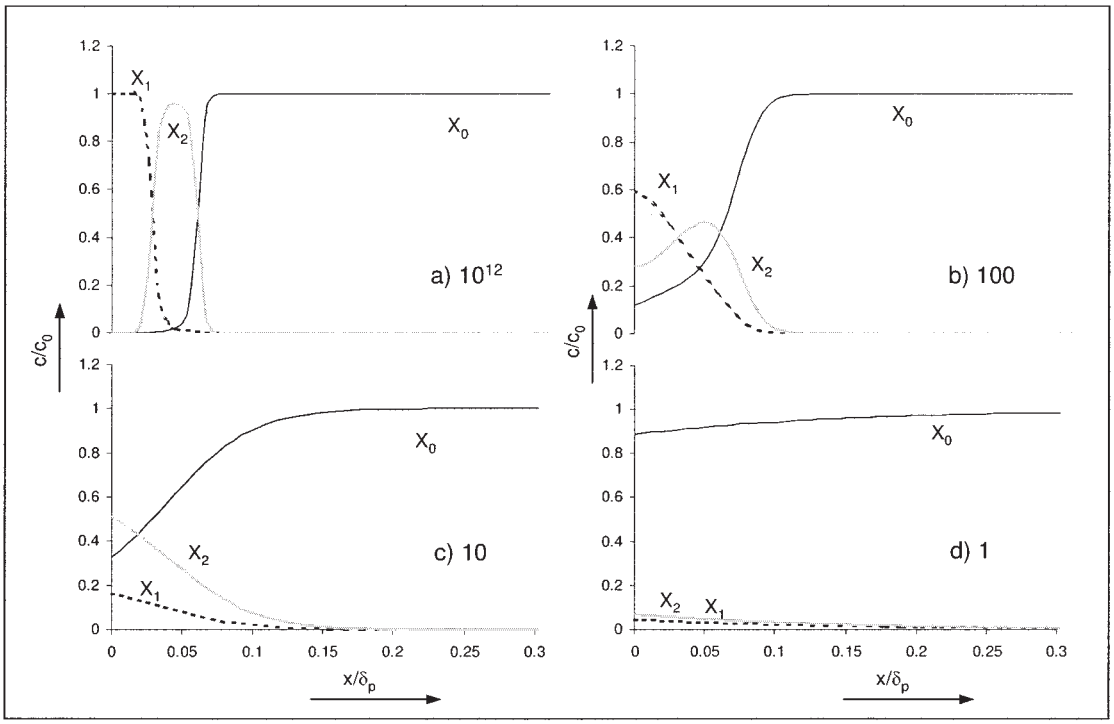

Figure 13. Concentration profiles for $k_3 = 10^6$ m^3/kmol/s with varying values of K_{15} and K_{24} as indicated.

rate-determining step. The shifting of enhancement factors with k_3 as shown in Figure 12 also occurs with other reaction rate constants. In the following examples, k_2, k_3, and k_4 have been fixed at various values so as to keep the equilibrium between X_1 + B and X_2 constant.

In Figure 14 k_2, k_3, and k_4 are set to 10^{10}, creating a very fast equilibrium between X_1 + B and X_2 and a fast reaction from X_2 to X_1. The variation in k_5 ranges from 10^6 to 10^{11}. In Figure 14 the enhancement factor is shown as a function of k_1. The shape of the enhancement curves is similar to earlier observations, that is, Figures 4 and 12. Starting with $k_5 = 10^9$ s^{-1} and increasing, it is observed that the value of the enhancement factor becomes smaller at identical values of k_1. This is no surprise as an increase in the rate of R_5 has to be compensated by a higher rate for R_1 to maintain the equilibrium. For values of k_5 lower than 10^8 s^{-1}, there is no shift in the enhancement factors; in this regime the pathway towards X_0 is faster via X_2 (reaction R_2 and R_3) since the profiles for the concentration of B do not vary much as a function of k_5. The equilibrium constant of the reaction between X_0 and X_1 can be expressed as the ratio of k_1 and k_5, and from Figure 14 it is concluded that E_∞ is independent of the value of the equilibrium constant. This is in contrast to the findings of the reversible system A + B $\leftrightarrow$ P, where the E_∞ is a function of the equilibrium constant.[17] The major difference between the straightforward reversible system and the reactions of the HC model is that in the latter system one reaction is irreversible; therefore, the catalytic cycle is not fully reversible and cannot be represented by a single equilibrium from which the catalytic intermediates are eliminated.

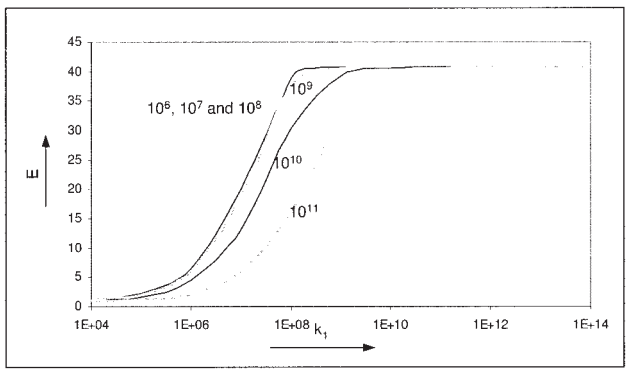

Figure 14. Enhancement factor as a function of the rate constant for the reaction X_0 + A $\rightarrow$ X_1 for various values of k_5 (indicated near the lines; k_2, k_3, and k_4 are equal to 10^{10}).

The diffusivity of the catalytic intermediates also influences the extent of the E_∞, as is shown in Figure 15. In line with the simulations of Figure 10, the diffusion coefficients of the catalytic intermediates have been lowered in alternating fashion. The values for the rate constants other than given in Figure 15 were set at $k_1 = 10^{14}$ m^3/kmol/s and $k_5 = 10^6$ s^{-1}, making the reaction between X_0 and A very fast and irreversible. The diffusion coefficients of the components and the other catalytic intermediates were kept constant at 10^{-9} m^2/s. As is clear from Figure 15, E_∞ depends on the value of k_3. For the lower k_3, it is observed that the E_∞ for a lower $D_c(X_0)$ decreases and E_∞ increases with lower $D_c(X_1)$ and $D_c(X_2)$, while between the latter two also a small difference exists. This is in line with the findings in the irreversible system so it is likely that the mechanisms leading to these observations must be similar. Decreasing $D_c(X_0)$ has the effect that the concentrations X_1 and X_2 near the G/l interface decrease; on the other hand, decreas-

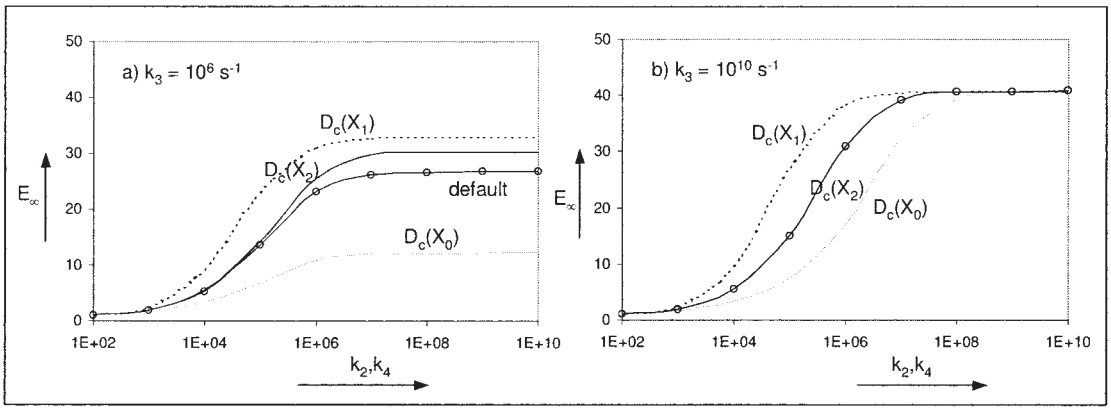

Figure 15. Enhancement factor at infinitely fast reaction for $X_0 + A \rightarrow X_1$ as a function of R_2 and R_4.

The default value is 10^{-9} m^2/s. Evaluated for diffusion coefficients of catalytic intermediates of 10^{-10} m^2/s.

ing $D_c(X_1)$ or $D_c(X_2)$ leads to effectively higher concentrations of the corresponding intermediates in the absorption region for A. When the concentration of X_2 changes, the reaction rate of R_3 changes; and because the value of k_3 is small compared to the other kinetic constants, R_3 is the rate-determining factor in the overall catalytic cycle. With k_3 equal to 10^{10}, the reaction R_3 is no longer the rate-determining step and E_∞ is only determined by the R_2/R_4 equilibrium. For high values of k_2 and k_4, there is no effect of the diffusivity of the catalytic intermediates because all the reaction steps in the cycle are very fast and a lower diffusivity of one of the intermediates is compensated by the others. For lower values of k_2 and k_4, the effects are identical to the observations with $k_3 = 10^6$ with the exception of the lower $D_c(X_2)$; the curve is exactly equal to the default case. While R_3 is very fast, X_2 is almost instantaneously converted to X_0 and since this intermediate has a default diffusion coefficient there is no net effect. For simulations with $D_c = 10^{-8}$ m^2/s, the results and effects are in line with those presented in Figure 15 and Figure 10 and, therefore, will not be discussed.

Conclusion concerning reversibility

The occurrence of reversible reactions in the catalytic cycle has a profound effect on the absorption rate of the gaseous reactant. Not only is the location of the equilibrium important, but also the rate of the equilibrium affects the absorption rate. The diffusion of the catalytic intermediates is just as important as with the irreversible reaction system; the explanation of the observed enhancement factors is more complicated than with irreversible reactions.

Simplified Models for Design

In the following section, it is assumed that the HC model represents the exact kinetic mechanism of a virtual process. The results from the simplified ABP and Bo models will be reflected on the predictions for the HC model. It must be noted, however, that the scheme ABP is the exact representation of the irreversible molecular reaction scheme without homogeneous catalysis.

Bo model

In the simulations with the HC model leading to the results shown in Figure 14, the effect of K_{15} on the absorption rate has been studied in relation to the other reaction rates. These simulations have been repeated with the Bo model. Since both models have identical kinetic parameters, the calculated enhancement factors can be directly compared. The fit of the Bo model in the range of applied parameters agrees very well to the results of the HC model. The average deviation between the E-values is 0.16% while the maximum observed deviation is 0.30%. As was noticed from the results shown in Figures 10 and 11, differences in diffusion coefficients can have significant influence on the total concentration distribution of the catalytic intermediates as well as on the enhancement of the rate of absorption. In the Bo model the intermediate species have been eliminated out of the kinetic rate expressions by application of the Bodenstein principle.

To study the diffusion effects, the results for the Bo model are compared with the E_∞ values obtained with the HC model in Figure 15. Because the results for the Bo model match the default ($D_c = 10^{-9}$ m^2/s) case of the HC model very well, Figure 15 is not only a graph for the HC model with varying diffusion coefficients but represents the differences between the Bo and HC models as well. To express the differences in a more direct fashion, the equivalent parity plot is given in Figure 16. Figure 16 clearly indicates that for deviating diffusion coefficients, the Bodenstein approximation leads to erroneous enhancement factors. Only when the diffusion of the catalytic intermediates is not important (see the discussion in the paragraph on the effect of reversibility) does application of the Bodenstein approximation lead to accurate predictions.

ABP model

Despite having the most simple expression for the reaction rate, the results for the ABP model are more difficult to compare to the HC model because the models comprise different kinetic parameters. An approach to compare the ABP model with the HC model is derived from the observation that the characteristics of the Bo model lie between those of the ABP and HC models. Because of the very good match between

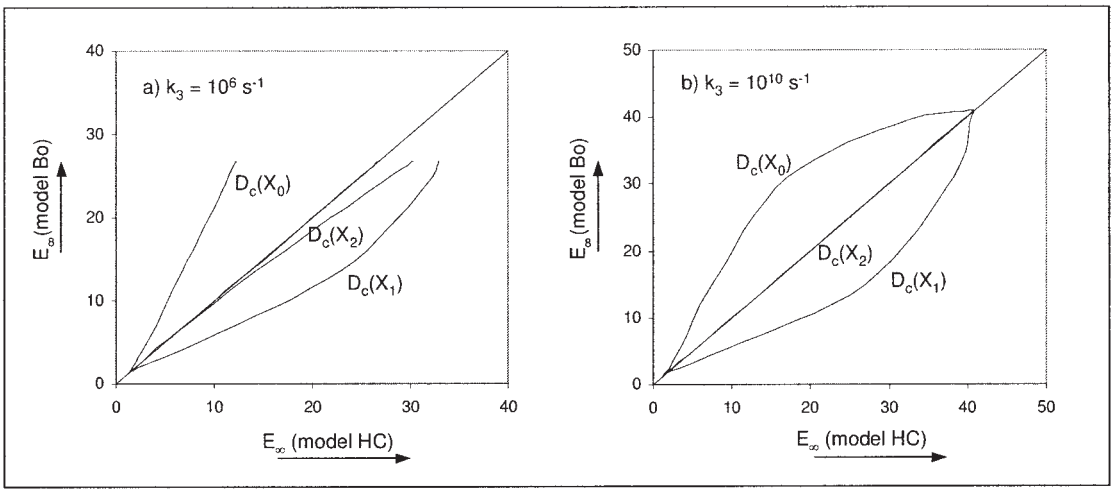

Figure 16. Parity plot of the enhancement factor at infinitely fast reaction for $X_0 + A \rightarrow X_1$ of the Bo model as a function of the values calculated by the HC model.

Evaluations for alternating lowered diffusion coefficients of catalytic intermediates compared to the default (default is 10^{-9} m^2/s, the lower value of 10^{-10} m^2/s is indicated by the labels).

the Bo model and the HC model, the results for the ABP model can be compared to both models. Through the proper choice of k_1 in the ABP model, the reaction rate calculated by the Bo model (see Eq. 4) matches the rate in the ABP model quite closely. For simplification, Eq. 4 is put in the form of:

$$R_i = \nu_i \cdot \frac{a_1 \cdot c_A \cdot c_B}{1 + a_2 \cdot c_A + a_3 \cdot c_B + a_4 \cdot c_A \cdot c_B}$$

with

$$a_1 = \frac{k_1 \cdot k_2 \cdot k_3}{k_5 \cdot (k_3 + k_4)} \cdot c_{cat}$$

$$a_2 = \frac{k_1}{k_5}$$

$$a_3 = \frac{k_2 \cdot k_3}{k_5 \cdot (k_3 + k_4)}$$

$$a_4 = \frac{k_1 \cdot k_2}{k_5 \cdot (k_3 + k_4)} \qquad (14)$$

Now, the k_1 in the ABP model can be chosen as:

$$k_1 = \frac{a_1}{1 + a_2 \cdot c_A^{ref} + a_3 \cdot c_B^{ref} + a_4 \cdot c_A^{ref} \cdot c_B^{ref}} \qquad (15)$$

The concentrations c_A^{ref} and c_B^{ref} are fixed reference concentrations. The choice for these concentrations determines the quality-of-fit between the reaction rate calculated by the Bo model and the ABP model, respectively, but the extent of this influence is variable because it depends on the value of the rate constants in the Bo model. (In the extreme when a_2 to a_4 are so small that all factors are much smaller than unity in the denominator of Eq. 15, the choice of c_A^{ref} and c_B^{ref} is arbitrary.) The enhancement factor as a function of k_1 for the ABP model is shown in Figure 4, so when k_1 has been calculated according to Eq. 15 the enhancement factor for the ABP model is known and can directly be compared with E calculated for the Bo model. The simulations performed with the HC model have been repeated with the ABP model in addition to the already performed simulations with the Bo model. After a few trials the reference concentrations were fixed at $c_A^{ref} = 0.025$ kmol/m^3 and $c_B^{ref} = 1.0$ kmol/m^3 (that is half of the values for the interfacial respectively the bulk liquid concentration). The results for enhancement factors with the ABP model compared to the Bo model are shown in Figure 17. The curve for E_∞ with all the diffusion coefficients equal to the default values of 10^{-9} m^2/s as performed with the HC model (shown in Figure 15) repeated with the ABP model with unaltered references gives also a reasonable agreement; the average difference in E-values is 7%, with a maximum deviation of 20%.

Conclusion concerning model simplification

The Bodenstein approximation simplifies the HC model to a large extent while the quality of the predictions remains very good. Only in case of changes in physical parameters that are not intrinsically present within the Bo model does the fit of the Bo model decrease. With the even more simple ABP model, the range in which accurate simulations for the HC model are provided is limited, but the flexibility is good.

Conclusions

The mass transfer of a gaseous reactant into a liquid where the reactions are catalyzed by homogeneous catalysts still offers challenges for chemists and chemical engineers. In this article the diffusion-reaction equations according to Higbie's penetration theory have been numerically solved. The catalytic cycle of the reaction network comprised two equilibria and one irreversible reaction.

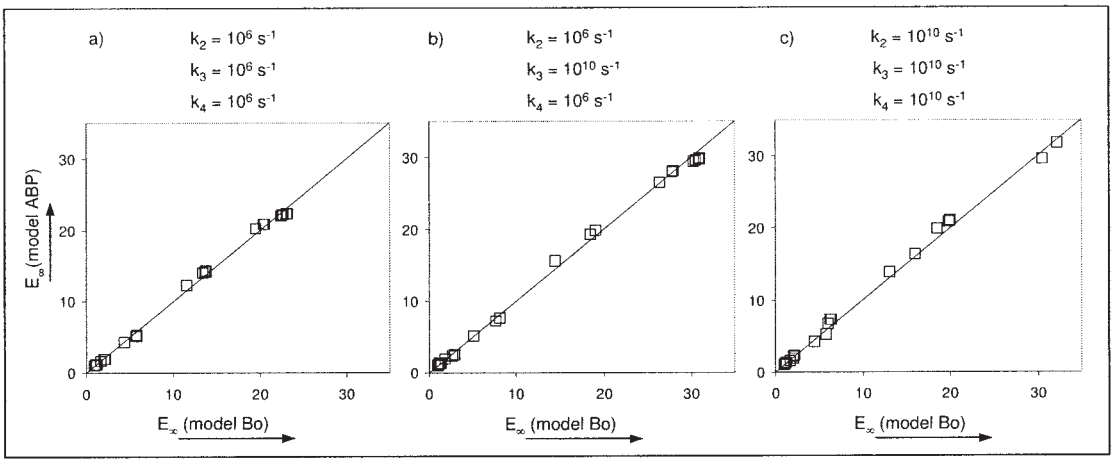

Figure 17. Parity plots of the enhancement factor for the reaction A + B → P of the ABP model versus the Bo model.

Evaluations for varying values of k_1 ($10^2..10^{14}$ m^3/kmol/s) and k_5 ($10^6..10^{11}$ s^{-1}), $c_A^{ref} = 0.025$ kmol/m^3 and $c_B^{ref} = 1.0$ kmol/m^3.

The least complicated case to study is when the equilibria are replaced with irreversible reactions. By varying a limited number of reaction rate constants, several effects on the absorption rate of A have been observed. The variation of reaction rate constants determines the concentrations of all components including the catalytic intermediates and with the concentrations the enhancement of the absorption can be explained. In addition to the kinetics also diffusion can be involved, for example, in the case of differences in the diffusivity of the catalytic intermediates.

The occurrence of reversible reactions in the catalytic cycle has a profound effect on the absorption rate of the gaseous reactant. Not only is the location of the equilibrium important, but also the rate at which the equilibrium is established affects the absorption rate. The importance of the diffusion of the catalytic intermediates is comparable to the irreversible reaction system; however, the explanation of the shifts in enhancement factors is more complicated.

Once a rigorous model for absorption with homogeneously catalyzed reactions has been obtained, the verification of simplified model versions is not difficult. It has been shown that with the Bodenstein approximation, very good predictions for the absorption rates are obtained for a wide range of kinetic parameters. When the rigorous model contains physical parameters not included in the Bodenstein model, the predictions are less reliable as, for example, in the case of deviating diffusivities of the catalytic intermediates. The simple model A + B → P can be tuned to match the absorption rates as well as the Bodenstein model, but the range of application for the parameters is limited. Simplification of systems of homogeneously catalyzed reactions with mass transfer by means of incorporation of the catalyst concentration into the reaction rate constant could easily result in the prediction of erroneous absorption rates.

The catalytic system applied in this study is quite simple and extension of the reaction networks is one of the points of interest for further research. Also, more complicated interactions of the catalytic intermediates, such as ligand exchanges and deactivation, are interesting from an industrial point of view. Finally, the study of the behavior of a fully reversible catalytic cycle is the next step to be performed.

Notation

c = concentration
D, D_c = diffusion coefficient
E = enhancement factor
E_∞ = enhancement factor at infinitely fast reaction
J = flow across gas-liquid interface
k = reaction rate constant
k_g = gas side mass transfer coefficient
k_L = liquid side mass transfer coefficient
mgl = solubility coefficient defined as c_{liquid}/c_{gas}
R = reaction rate
t = time variable
x = spatial variable

Greek symbols

δ_p = penetration depth
φ = Hatta number
τ_p = contact time

Indices

bulk = liquid bulk
gas, liquid = phase
cat = catalyst
i = any component
j = any reaction
$*$ = at the interface, at equilibrium

Components

A = gas phase reactant
B = liquid phase reactant
P = liquid phase product
X_0 = catalytic complex
X_1 = catalytic complex
X_2 = catalytic complex

Literature Cited

1. Halpern J. Mechanistic aspects of homogeneous catalytic hydrogenation and related processes. *Inorg Chim Acta.* 1981;50:11-19.
2. Halpern J, Wong CS. Hydrogenation of tris(triphenylphosphine)chlororhodium(I). *J Chem Soc Chem Comm.* 1973;629-630.
3. Halpern J, Okamoto T, Zakhariev A. Mechanism of the chlorotris(triphenylphosphine) rhodium(I) catalyzed hydrogenation of alkenes. The reaction of chlorodihydridotris-(triphenylphosphine)rhodium(III) with cyclohexene. *J Mol Cat.* 1976;2:65-68.

4. Sanchez-Delgado RA, Rosales M. Kinetic studies as a tool for the elucidation of the mechanisms of metal complex-catalyzed homogeneous hydrogenation reactions. *Coor Chem Rev.* 2000;196:249-280.
5. Zang V, van Eldik R. Reaction kinetics of iron chelates with sulfur oxides and nitrogen oxides in aqueous solution: waste gas purification by homogeneous catalysis? *DECHEMA Monographien*. 1989;118: 143-156.
6. Cavalieri d'Oro P, Raimondi L, Pagani G, Montrasi G, Gregorio G, Adreetta A. Propene hydroformylation with rhodium carbonyls and triphenylphosphine. II—Kinetics of butyraldehydes formation. *La chimica e l'industria.* 1980;62:572-579.
7. Kelkar AA, Jaganathan R, Chaudhari RV. Hydrocarbonylation of methyl acetate using a homogeneous Rh(CO)Cl(PPh3)2 complex as a catalyst precursor: kinetic modeling. *Ind Eng Chem Res.* 2001;40: 1608-1614.
8. van Elk EP, Borman PC, Kuipers JAM, Versteeg GF. Modelling of gas-liquid reactors—stability and dynamical behaviour of a hydroformylation reactor. *Chem Eng Sci.* 2001;56:1491-1500.
9. van Swaaij WPM, Versteeg GF. Mass transfer accompanied with complex reversible chemical reactions in gas-liquid systems: an overview. *Chem Eng Sci.* 1992;47:3181-3195.
10. Ponzi EN, Lemcoff NO. Influence of mass transfer on homogeneous catalytic gas-liquid reactions. *Rev Latinoam Ing Quim Apl.* 1981;11: 1-12.
11. Hoorn JAA, Versteeg GF, Modelling of mass transfer and reaction: diffusion effects of radical intermediates. Submitted for publication to *Chem Eng Sci*.
12. Helfferich FG. "Kinetics of homogeneous multistep reactions," *Comprehensive Chemical Kinetics, Vol. 38*, Compton RG, Hancock G, eds. Amsterdam: Elsevier; 2001:283-286.
13. Versteeg GF, Blauwhoff PMM, van Swaaij WPM. The effect of diffusivity on gas-liquid mass transfer in stirred vessels. Experiments at atmospheric and elevated pressures. *Chem Eng Sci.* 1987;42:1103-1119.
14. Westerterp KR, van Swaaij WPM, Beenackers AACM. *Chemical Reactor Design and Operation*. New York: John Wiley & Sons; 1990:357-494.
15. Cornelisse R, Beenackers AACM, van Beckum FPH, van Swaaij WPM. Numerical calculation of simultaneous mass transfer of two gases accompanied by complex reversible reactions. *Chem Eng Sci.* 1980;35:1245-1260.
16. Baker GA, Oliphant TA. An implicit, numerical method for solving the two-dimensional heat equation. *Quart Appl Math.* 1960;17:361-373.
17. Versteeg GF, Kuipers JAM, van Beckum FPH, van Swaaij WPM. Mass transfer with complex reversible chemical reactions—I. Single reversible chemical reaction. *Chem Eng Sci.* 1989;44:2295-2310.

Appendix: Bodenstein Approximations

The reaction rates R_i are defined in Figure 3.

$$\text{Assume steady state for } X_1: \quad R_2 + R_5 = R_1 + R_4 \tag{A1}$$

$$\text{Assume steady state for } X_2: \quad R_2 = R_3 + R_4 \tag{A2}$$

Substitute the expressions for R_i:

$$k_2 \cdot c_B \cdot c_{X_1} + k_5 \cdot c_{X_1} = k_1 \cdot c_A \cdot c_{X_0} + k_4 \cdot c_{X_2} \tag{A3}$$

$$k_2 \cdot c_B \cdot c_{X_1} = k_3 \cdot c_{X_2} + k_4 \cdot c_{X_2} \tag{A4}$$

Combine Eqs. A3 and A4 and rearrange:

$$c_{X_0} = \frac{1}{k_1 \cdot c_A} \cdot \left\{ k_5 \cdot \frac{k_2 \cdot k_3 \cdot c_B}{k_3 + k_4} \right\} \cdot c_{X_1} \tag{A5}$$

Total catalyst concentration constant and equal to c_{XT}:

$$c_{XT} = c_{X_0} + c_{X_1} + c_{X_2} \tag{A6}$$

Substitute Eqs. A4 and A5 in A6:

$$c_{X_1} = \frac{c_{XT}}{1 + \frac{k_5}{k_1} \cdot \frac{1}{c_A} + \frac{k_2 \cdot k_3}{k_1 \cdot (k_3 + k_4)} \cdot \frac{c_B}{c_A} + \frac{k_2}{k_3 + k_4} \cdot c_B} \tag{A7}$$

Transferring Eq. A7 into the reaction rate expression R_1 and some straightforward rearrangements gives Eq. 4:

$$R_i = \nu_i \cdot \frac{\frac{k_1 \cdot k_2 \cdot k_3}{k_5 \cdot (k_3 + k_4)} \cdot c_A \cdot c_B \cdot c_{XT}}{1 + \frac{k_1}{k_5} \cdot c_A + \frac{k_2 \cdot k_3}{k_5 \cdot (k_3 + k_4)} \cdot c_B + \frac{k_1 \cdot k_2}{k_5 \cdot (k_3 + k_4)} \cdot c_A \cdot c_B}$$

with $\nu_i = -1$ for i = A,B and $\nu_i = 1$ for i = P.

Manuscript received Sept. 26, 2005, and revision received Mar. 17, 2006.